An intra-domain allosteric network modulates the calcium affinity of the C-type lectin receptor Langerin

Jonas Hanske[†,‡,⊥], Stevan Aleksić[‡,⊥], Martin Ballaschk[‡,§,#], Marcel Jurk[‖], Elena Shanina[†,‡], Monika Beerbaum[§], Peter Schmieder[§], Bettina G. Keller[*,‡], Christoph Rademacher[*,†,‡]

[†]Max Planck Institute of Colloids and Interfaces, Dept. of Biomolecular Systems, Am Mühlenberg 1, 14476 Potsdam, Germany

[‡]Freie Universität Berlin, Institute of Chemistry and Biochemistry, Dept. of Biology, Chemistry, and Pharmacy, Takustr. 3, 14195 Berlin, Germany

[§]Leibniz-Institut für Molekulare Pharmakologie, Robert-Rössle Str. 10, 13125 Berlin, Germany

[‖]Max Planck Institute for Molecular Genetics, Dept. of Bioinformatics, Ihnestraße 63-73, 14195, Germany

Allostery, molecular dynamics, metal-binding protein, protein dynamics, mutual information.

ABSTRACT: Antigen uptake and processing by innate immune cells is crucial to initiate the immune response. Therein, the endocytic C-type lectin receptors serve as pattern recognition receptors detecting pathogens by their glycan structures. Herein, we studied the carbohydrate recognition domain of Langerin, a C-type lectin receptor involved in the host defense against viruses such as HIV and influenza as well as bacteria and fungi. Using a combination of nuclear magnetic resonance and molecular dynamics simulations, we unraveled the molecular determinants underlying cargo capture and release encoded in the receptor architecture. Our findings revealed receptor dynamics over several timescale associated with binding and release of the essential cofactor Ca^{2+} controlled by the coupled motions of two loops. Applying mutual information theory and site-directed mutagenesis, we identified an allosteric intra-domain network that modulates the Ca^{2+} affinity depending on the pH thereby promoting fast ligand release.

Introduction

Many members of the protein family of C-type lectin receptors (CLRs) serve as transmembrane or secreted pattern recognition receptors of the innate immune system and play an important role in regulating the immune response. This pathogen recognition process is based on defined glycan structures present on the surface of the pathogen and in case of membrane-bound receptors recognition can lead to uptake and successive antigen processing and presentation.[1] A central Ca^{2+} ion that is coordinated by a cage of charged amino acid side chains of the carbohydrate recognition domain (CRD) is the mediator of this interaction (**Figure 1A**) and thereby ultimately key element in regulating the uptake and routing of the cargo to the endosomal compartment. While the extracellular milieu provides stable Ca^{2+} concentration and pH, acidification and active Ca^{2+} export in the early endosome highly reduce the carbohydrate affinity resulting in cargo release Consequently, every step from the initial contact, triggering the uptake to cargorelease and sorting, and in some cases receptor recycling, is tightly controlled. The architecture of CLRs reflects this demand of an adaptive ligand binding module with a remarkable evolutionary flexibility to keep up with co-evolving pathogens.[2]

While the pH dependency for both carbohydrate ligands and Ca^{2+} binding has been reported for several CLRs such as DC-SIGN, DC-SIGNR, and the hepatic receptor ASGPR [3-6], limited structural data is available on the molecular mechanisms underlying the important determinants of cargo uptake and release. Two such determinants have been associated with cargo release upon acidification of the receptor environment. Firstly, some oligomeric CLRs lose their multimerization state resulting in decreased avidity.[7] Secondly, the protonation of the amino acids of the Ca^{2+} cage release the ion and abrogate carbohydrate interaction: For the ASGPR, a central histidine residue acts as pH sensor whose sidechain protonation state controls Ca^{2+} affinity.[5,8,9] However, pH dependence of binding is not universal for all CLRs and even closely related family members show differential behavior such as DC-SIGN, DC-SIGNR and LSECtin, wherein only the former two proteins show pH dependence binding.[4] For DC-SIGNR, a decrease in pH results in structural or dynamics changes and a partial release of Ca^{2+},[10] but the underlying molecular mechanisms remain elusive. Large conformational changes of the CRD are associated with Ca^{2+} release in almost all cases for which a structure has been solved in absence of the Ca^{2+} in the canonic carbohydrate binding site. A conserved proline, located in the

central long loop harboring this site, switches back from cis to trans conformation.[8,11-14] For the mannose-binding protein (MBP) this mechanism was proposed to serve as a kinetic trap, preventing rebinding of the cargo allowing separation of recycling receptors and lysosomal degradation of the payload.[12]

The trimeric CLR Langerin is a pattern recognition receptor mainly found on Langerhans cells.[15,16] It is involved in the detection of a wide set of pathogens including viruses such as HIV,[17] measles,[18] and influenza virus,[19] as well as fungi[20] and mycobacteria,[21] and recognizes antigens of endogenous origin such as H and B blood group antigens[22] and heparin.[23,24] Langerin harbors a single Ca^{2+} site[25] embedded in the canonical EPN motif that conveys mannose-type monosaccharide specificity. Langerin is a recycling endocytic receptor that releases its cargo in the early endosome while the receptor itself accumulates in $Rab11^{+}$ recycling compartments.[15,26] Upon acidification, Langerin remains in trimeric form.[27] Langerin-mediated antigen uptake is of particular interest as it has been shown to allow for presentation of exogenous peptide antigens to both $CD8^{+}$ and $CD4^{+}$ T-cells.[28,29]

We therefore set out to elucidate the determinants for Ca^{2+} binding and release and applied nuclear magnetic resonance (NMR) and isothermal titration calorimetry (ITC) in combination with molecular dynamics (MD) simulation. We demonstrated Ca^{2+} binding is pH dependent whereas the effect of acidification on carbohydrate recognition is limited. We attribute the fine-tuning of the Ca^{2+} affinity to a robust and pH sensitive allosteric network that couples the motions of the binding loop with an adjacent small loop. We identified H294 as a partial pH sensor. This histidine however does not coordinate Ca^{2+} directly but instead is a central hub of the allosteric network which couples the two loops. The proposed mechanism is distinctively different from the two known mechanisms of Ca^{2+}-affinity control in that it does not rely on a single (switch-like) structural change, but the flexibility of the entire binding loop regulates Ca^{2+} affinity which is in turn regulated by an extended allosteric network. Thus, the receptor architecture does not only serve as a scaffold for the carbohydrate binding site but takes an active role in cargo uptake and release.

Results

Carbohydrate binding to Langerin is Ca^{2+}-dependent while Ca^{2+} affinity itself is pH-dependent

To investigate the structural determinants of cargo binding and release, we first analyzed the pH dependence of carbohydrate binding to human Langerin extracellular domain (ECD). The affinity to mannan, a natural fungal polysaccharide ligand, dropped rapidly with decreasing pH with a half-maximum at pH 5.4±0.1 and abolished below pH 5 in accordance with previous reports (**Figure 1B**).[27] To further dissect whether this loss of binding was due to decreased affinity for the carbohydrate ligand itself or for the central Ca^{2+} coordinating the glycan, we determined the dissociation constants for mannose as a simple monovalent ligand and the essential cofactor Ca^{2+} at both pH 7 and pH 6 by ITC **(Figure 1C-F)** for the CRD. Additional ^{1}H-^{15}N HSQC NMR titrations confirmed these results (**Figure S1**) The affinity for mannose decreased slightly from 6.2±0.5 mM to 9.2±1.2 mM at saturating Ca^{2+} concentrations at pH 6 and 7, respectively. However, the affinity for Ca^{2+} dropped significantly from 120±65 μM to 800±150 μM (**Figure 1C, E**). Moreover, at pH 7, CRD and ECD share almost identical affinities for both Ca^{2+} and mannose (**Figure 1D**). Thus, it can be assumed that there is no major inter-domain cooperative behavior involved in the recognition of simple monovalent ligands.

The pH-dependence of Ca^{2+} affinity is likely under intra-domain allosteric control

Surprisingly, during NMR titrations experiments we observed pronounced changes in chemical shifts of many resonances at both pH 6 and 7, which was unexpected for a rigid protein with a single binding site (**Figure 2A**). To gain structural insight, 92% of the backbone resonances of the holo form of Langerin CRD at pH 6 were assigned (**BRMB entry: 26791**, **Figure S2**). The long loop and the β4-strand remained unassigned presumably due to unfavorable dynamics of this region as observed for other CLRs.[31,32] We identified 43 residues at pH 6 and 48 at pH 7 outside a 5 Å radius of the binding site that were affected by Ca^{2+} binding (**Figure 2C**). As these two sets were 95% identical we concluded that the same residues being involved in Ca^{2+} binding at both pH. These perturbations are located predominantly in proximity of the glycan binding site with the most prominent effects in the β2 and β2' strand and the enclosed short loop (residues 255-265) (**Figure 2C**). Intriguingly, these amino acids were pH responsive in the holo form (**Figure S3A**). Closer inspection of the chemical shift changes revealed that the small loop in the holo form has distinct conformations at pH 6 and pH 7 (**Figure S3B-D**). Analysis of 28 mammalian Langerin homologs revealed a significant higher evolutionary conservation of those residues compared to the rest of the sequence (**Figure 2C, Figure S4**) indicative of a conserved function.

Moreover, we observed that many peaks undergo severe line broadening during Ca^{2+} titration at both pH, which is indicative for intermediate fast exchange on the NMR timescale that might be caused by slow kinetics of binding and allosteric structural rearrangements on the micro- to millisecond timescale[33] (**Figure S5A**). This observation might explain the deviations between the dissociation constants determined from ITC and NMR (**Figure S5B**).[34] Taken together, we found that pH-dependent ligand release is dominated by decreased Ca^{2+} affinity. In turn, Ca^{2+} binding affects a large network of residues in a pH dependent manner indicating an allosteric control mechanism.

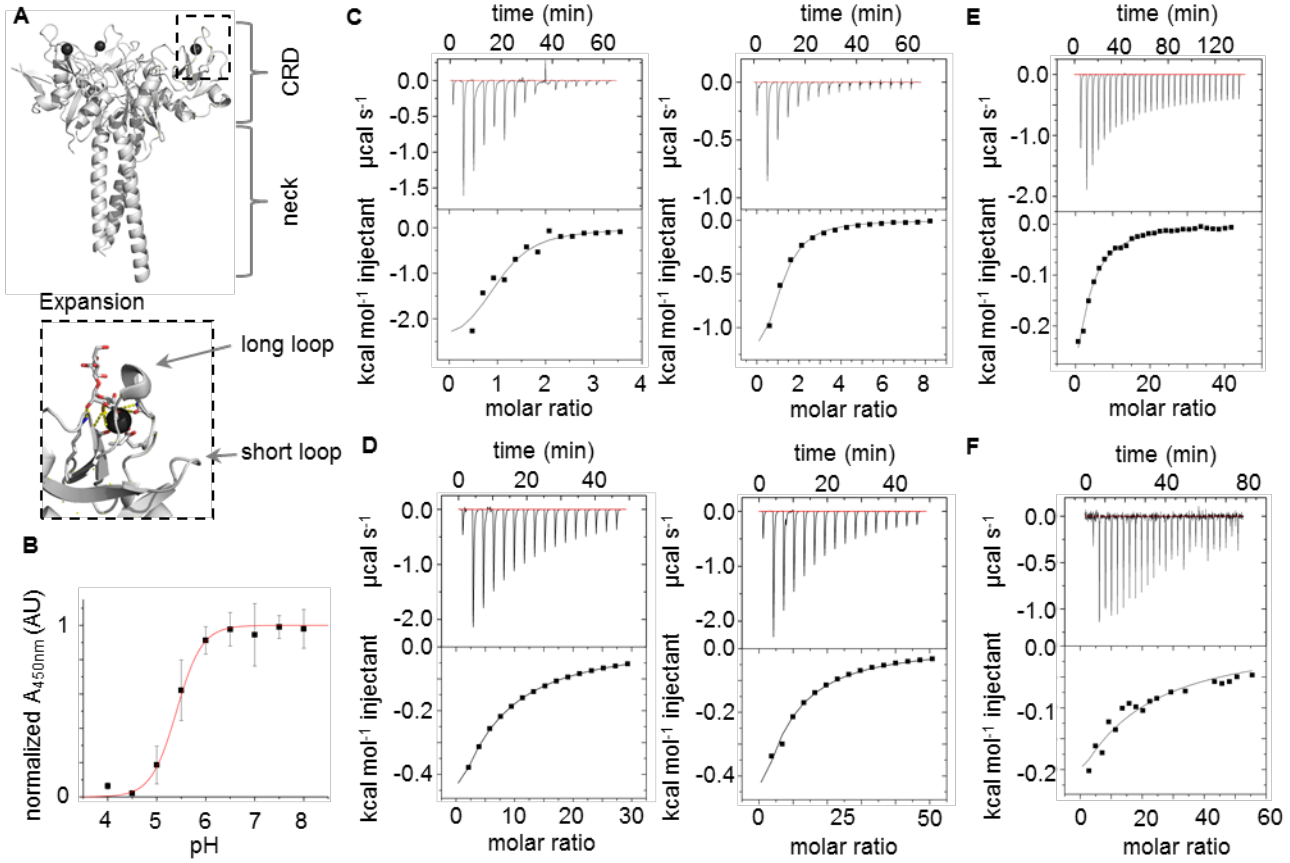

Figure 1: Ca^{2+} binding of Langerin is highly pH dependent. (A) Cartoon representation of trimeric Langerin ECD (pdb entry: 3KQG{Feinberg, 2010 #7}) and expansion of binding site with complexed Ca^{2+} and dimannoside fragment (pdb entry: 3P5D{Feinberg, 2011 #28}) (B) Binding of Langerin ECD to mannan-coated plates decreases rapidly upon acidification with a pH_{50} of 5.4±0.1 and a Hill coefficient of 1.7±0.3 (n=3, SEM as error bars). (C) ITC thermogram of Ca^{2+} interacting with Langerin CRD and ECD at pH 7 revealing the same affinity for Ca^{2+} with a K_d of 105±15 µM and 130±50 µM, respectively. (D) ITC thermogram of mannose interacting with Langerin CRD and ECD at pH 7. Again, both proteins have similar affinities with a K_d of of 6.2±0.5 mM and 5.6±1.5 mM, respectively. (E) ITC thermogram for Ca^{2+} binding to Langerin CRD at pH 6 (K_d = 800±150 µM) and (F) to mannose (K_d = 9.2 ± 1.2 mM). All measurements were conducted in triplicates at 298 K and stoichiometry was fixed to 1.

Apo Langerin CRD undergoes pH-independent prolyl cis trans isomerization

CLR Ca^{2+} coordination is governed by a cis/trans isomerization of a conserved proline of the EPN motif in the long loop forming the Ca^{2+} binding site[8,11-14]. To exclude that changes in cis/trans isomerization account for the observed differences in affinity at both pH, we analyzed the isomerization state of the long loop (residues 283-295). The ^{1}H-^{15}N HSQC spectrum of the Ca^{2+} unbound form (apo) showed additional peaks which we could attribute to the trans state of P286 in slow exchange with the help of a P286A mutant. We assigned 22 resonances of the trans state (**Figure S6A**). Notably, many of the resonances corresponding to the cis state of these interchanging residues experience significant chemical shift changes upon addition of Ca^{2+} (**Figure 2B**) substantiating our previous observation of an extended network of communicating residues.

Surprisingly, the average ratio of the peak intensities of the cis and trans showed that 75±10% of the apo form are in cis prolyl bond conformation (**Figure S6B**), which is in contrast to other CLRs where the majority of the apo population is found in trans.[8,11-14] Moreover, the cis/trans ratio and the chemical shift differences between the two states were unaffected by pH (**Figure S6C**) and do not explain the affinity differences upon acidification. Based on the ^{15}N chemical shift differences, we estimated an upper limit for the exchange rate of 1 s^{-1} (Table S1).[12]

Furthermore, upon addition of Ca^{2+}, only the resonances of the cis form shifted while the volume of the peaks of the trans form decreased. Hence, we conclude that only the cis form binds Ca^{2+}. These data are in line with previous reports on CLRs only with the prolyl bond in cis conformation being Ca^{2+} binding competent.[35,36] Additionally, these data suggest that the apo trans form is in slow exchange with the holo cis form, likely via the apo cis form. Thus, the decrease in trans population is caused by a shift of the equilibrium towards the holo cis form under saturating Ca^{2+}-concentrations. Taken together, the cis prolyl conformational state of Langerin is in slow exchange and

is highly preformed independent of pH and thus does not explain the pH-dependent affinity drop.

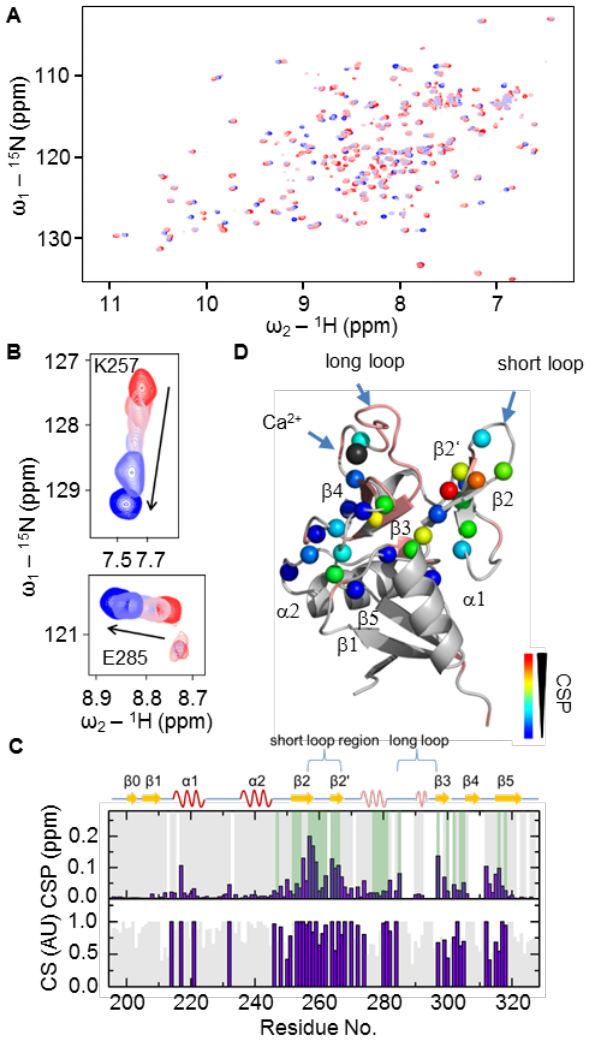

Figure 2: Ca^{2+} binding affects several residues remote from the binding site (A) Overlay of ^{1}H-^{15}N HSQC NMR spectra of apo and holo Langerin CRD at pH 6 and pH 7 at 298 K (holo forms are labeled in blue shades and apo forms in red shades, pH 6 forms are labeled in the stronger color hue). (B) Spectra expansions of K257 and E285 backbone resonances at increasing Ca^{2+} concentrations from 0 to 10 mM at pH 6 in intermediate exchange regime. (C) (top) Chemical shift perturbations induced by addition of Ca^{2+} at pH 6. Assigned residues and resonances in slow exchange in the apo form are highlighted grey and green, respectively. (bottom) Evolutionary conservation of allosteric network residues (labeled purple) among 26 mammalian species is significantly higher than of the residues that do not participate in the network (grey) ($p<0.005$, paired Wilcoxon signed ranks test). (D) Amino acids affected by Ca^{2+} addition (CSP>0.02 ppm) highlighted on the Langerin structure (pdb entry: 3P5F, color-coded according to the CSP, unassigned residues are colored salmon).

Langerin shows increased nanosecond dynamics in the small and long loop

In the absence of an X-ray crystal structure of the apo form and because the long loop was unresolved by NMR, we turned to MD simulations to gain more insight on how such large chemical shift perturbations could propagate from the Ca^{2+} binding site. We performed microsecond all-atom simulations in explicit water for all structures in the Ca^{2+}-binding equilibrium at pH 7: cis apo, cis holo, and trans apo Langerin. Excellent agreement between MD simulations and NMR data was demonstrated by comparing chemical shifts and $^{3}J_{HNHA}$ coupling constants for both cis apo and holo forms (**Figure S7**).

The overall structure of the cis apo form is highly similar to the structure of the cis holo form. Both simulations showed a rigid protein backbone where only the small loop exhibited increased backbone dynamics (**Figure 3A,B**). Additionally, the α3-helix became destabilized in the cis apo form. Although the trans apo form also showed a largely rigid backbone, the long loop sampled a distinctively different conformational space than in the two cis forms (**Figure 3C**). The latter simulation also showed that Ca^{2+} binding is sterically prohibited in the trans form confirming the NMR analysis. The large chemical shifts upon Ca^{2+}-binding of residues remote from the Ca^{2+}-binding site (found both in MD and in NMR) could be attributed to mostly minor local structural changes. For example, in the crystal structure the backbone torsion angles of D263 are in the β-sheet conformation (shown in gray in **Figure 3C**). This conformation is sampled in both apo and holo form. However, in the apo form, additionally the α-helix region is populated**.** The chemical environment of the N-H bond of A258 differs drastically in these two conformations (**Figure 3C**). Thus, the observed chemical shift perturbation upon Ca^{2+} binding is due to the removal of the minor conformation from the ensemble.

We suspected that the dynamics of the short loop could be correlated to the mobility of the proximal long loop for two reasons: (i) the long loop directly interacts with the Ca^{2+} ion but the largest chemical shifts upon Ca^{2+} binding occur in the small loop; and (ii) if Ca^{2+} is indeed under allosteric control, other flexible regions of the protein are likely involved. We tested this by computing autocorrelation functions of the distance between the two loops for several residue pairs. After a fast initial decay, the distance autocorrelation function decayed approximately exponentially with timescales of 5 to 6 ns. This was found for both the cis apo and the cis holo form (**Figure 3D**). This coupling on the nanosecond timescale is indicative of structural transitions that require a cooperative movement of the two loops. While this does not prove allostery in itself, it strongly hints at a pathway by which information (e.g. presence or absence Ca^{2+}) can be transmitted.

To gain more experimental insight into Langerin dynamics, NMR ^{15}N-backbone relaxation data at two field strength for both holo and apo form were acquired (**Fig-**

ure 3E, Figure S8A). Regardless of the presence of Ca^{2+}, we observed a pronounced reduction in the R_2 relaxation rate and the hetero NOE in the short loop compared to the remainder of the protein.

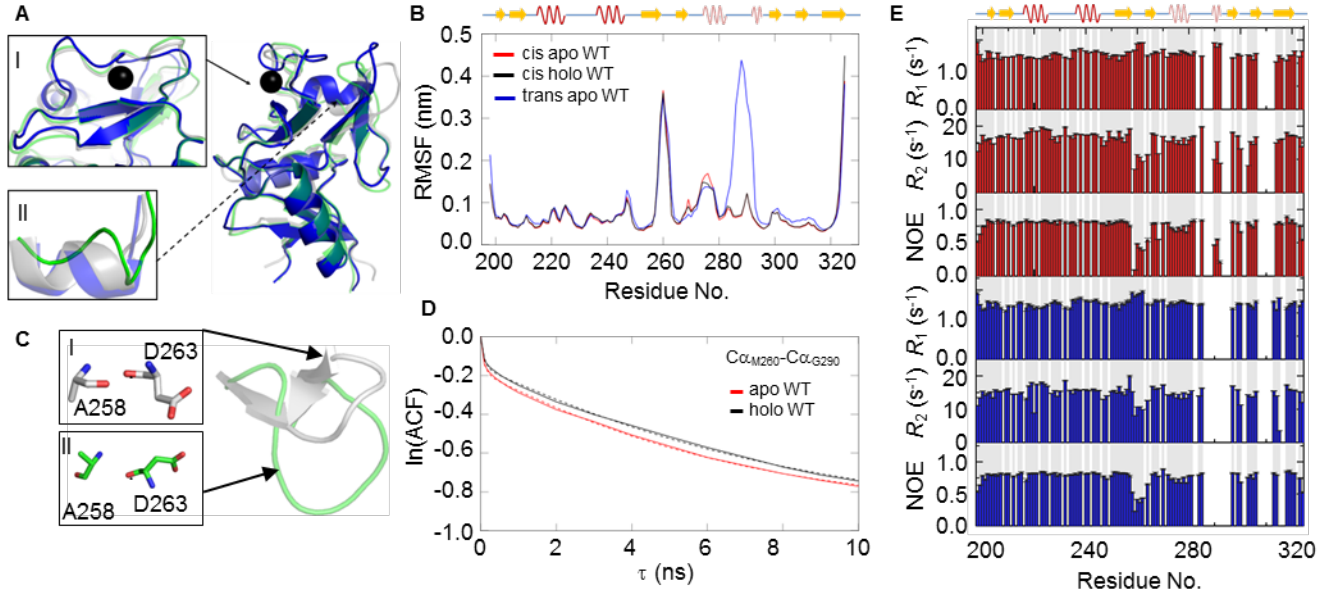

Figure 3: Conformational dynamics of the Langerin CRD is restricted to the long and the short loop. (A) Cartoon representation of the trans apo (blue), and cis apo (green) conformations superimposed to a Langerin crystal structure (grey, pdb entry 3P5H[37]) highlighting the altered conformational space in trans apo form (I) and the disordered α3-helix (II). (B) The root mean square fluctuations (RMSF) of the backbone nitrogen atoms averaged over the simulation (2μs) for the three Langerin CRD forms. Largest RMSF values are observed for residues of the short loop (residues 255-265) in all forms, while residues of the Ca^{2+} binding site undergo higher structural fluctuations only in trans apo form. (C) The chemical environment of A258 is perturbed by the changes in backbone flexibility of the adjacent amino acid D263. In the apo form, the short loop adopts a more opened conformation (green) compared to holo crystal structure (gray). Expansions I and II highlight the preferred conformations of A258 and D263 in the holo and apo form, respectively. (D) Autocorrelation functions calculated for the distance between Cα-atoms of M260 and G290. A double-exponential fit(dashed line) shows concerted mobility of the short and the long loop on the nanosecond timescale. (E) ^{15}N backbone relaxation rate constants R_1 and R_2 and hetero NOE of apo (red, upper panel) and holo (blue, lower panel) Langerin CRD (600 MHz, pH 6, 299 K). The protein exhibits uniform relaxation rate constants except in the short loop and long loop.

Model-free analysis of the relaxation data was unsuccessful likely due to major motions on slower timescales. However, the hetero NOE is sensitive to changes in local correlation times and can thus serve as a good estimate for internal motions. This reduction is therefore indicative for an increased mobility on the pico- to nanosecond timescale, which is in agreement with the conformational flexibility of the small loop in our simulations. In the apo form, an overall increase in R_2 rate constants compared to the holo form (16±3 s^{-1} vs. 15±3 s^{-1} at 600 MHz) as well as a field dependence of these rate constants of about 1 s^{-1} in both forms (**Table S2**) indicated the existence of dynamics on the micro- to millisecond timescale.[38]

Taken together, our MD simulation and experimental data are in good agreement and reveal that holo and apo Langerin CRD are structurally very similar and rather rigid with the exception of the short and the long loop region. In both forms the small loop moves correlated with the long loop on the nanosecond timescale indicating a coupling of the loop dynamics.

An allosteric network connects distal residues in Langerin and decreases Ca^{2+} affinity

Our observations strongly indicate an allosteric mechanism but do not directly prove its existence. Structural allostery exists if the conformations sampled by a region *A* depend on the current conformation in another region *B* of the protein. The mutual information directly measures to which degree the conformations in *A* are determined by the current conformation in *B*. It can directly be interpreted as the amount of information which is transmitted between the regions and has been used previously to detect allosteric networks in MD simulations of proteins.[39,40] We computed the normalized mutual information (NMI) between the ϕ-ψ torsion angle space (i.e. Ramachandran planes), between the ϕ-ψ torsion angle space and the side chain torsion angles χ, and between the side chain torsion angles of all pairs of residues. The results of the various NMIs per residue pair were added to obtain an aggregated measure for the inter-residue correlation revealing a common extended net-

work of correlated residues withinthe three structures of Langerin (cis apo, cis holo, trans apo) (**Figure 4; Figure S9**).

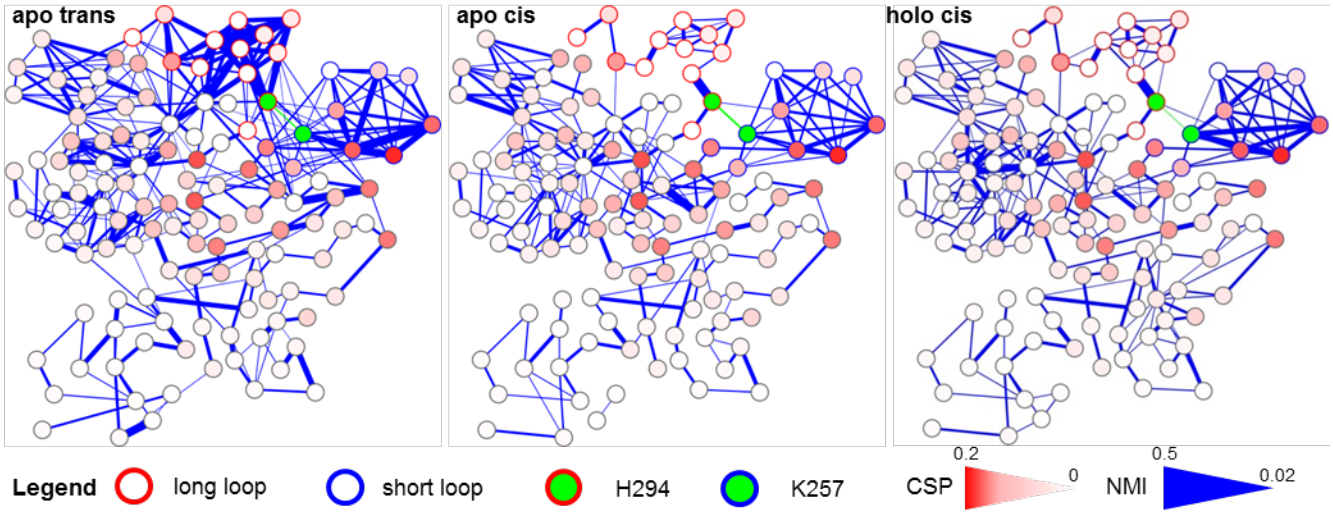

Figure 4: Mutual dependence graphs revealed correlated movement of the long and the short loop. Network representation of the mutual dependence graphs computed for the trans apo (left), cis apo (middle), and cis holo forms (right). Edge thickness corresponds to the aggregate NMI values (threshold 0.02). The edge between the hub residues H294 and K257 is highlighted (green). Nodes are colored according to CSP values observed upon Ca^{2+} binding. Nodes representing the long and short loop are marked redand blue borders, respectively. . The aggregated NMI values for H294-K257 decreases from 0.08 over 0.05 to 0.02 from left to right.

Furthermore, we found that the physical interactions underlying these correlated motions are propagated by a highly stable hydrogen bond network (**Figure S10**, **Table S1**). We mapped the residues that experienced chemical shift perturbations during Ca^{2+} titration (**c.f. Figure 2B**) to the same mutual information graph. Our findings emphasize a high similarity in connectivity, but deviate in the magnitude of the underlying correlations. These decrease when the system is shifted from trans to cis apo form, and further decreases in the fully Ca^{2+} bound holo form, suggesting an overall loss in correlation upon Ca^{2+} binding.

If such allosteric network existed, mutations should introduce perturbations that propagate through the network and result in chemical shift changes.[41] To probe the interaction between the long and short loop and their connection to other regions of the fold, ten mutants were prepared that were folded and bound Ca^{2+} as was observed by NMR (**Figures 5A andS11**). We quantified the chemical shift perturbations induced by mutation in their apo form with respect to the wild type (WT). For the majority of the mutants, perturbations were not restricted to the neighborhood of the mutation site but also affected remote residues. The perturbed residues typically were members of the network of correlated residues obtained from MD analysis (**Figure 5B, left**). Comparison of the holo forms of the mutant with the holo WT yielded the same picture for most mutants indicating that the network persists in the Ca^{2+} bound state (**Figure 5B, middle**). Finally, Ca^{2+} titration perturbed similar residues in most mutants compared to the WT lectin (**Figure 5B, right)** allowing for the definition of a robust core network of 24 amino acids (**Figure 5C**). Notably, H294A and K257A mutants binding to Ca^{2+} yielded a distinct pattern of chemical shift perturbations than in the WT with an about twofold reduction in the number of affected residues indicating that the allosteric network is corrupted in these mutants.

To assess whether the mutations also affected Ca^{2+} affinity, we determined the dissociation constants for seven mutants by NMR titrations at pH 6 (**Table 1, Figure S11**). Intriguingly, three mutants (H294A, K257A, K299A) showed increased affinity at pH 6 wherein H294A experienced the strongest effect (K_d = 110 µM). Since none of the mutants had an altered cis/trans isomerization of P286 at pH 6, we could exclude a contribution of the allosteric network to a conformational stabilization of either isomer at this pH (**Table S3**). Replacing K299 by alanine removes a positive charge in the vicinity of the Ca^{2+}-binding site, which explains the higher Ca^{2+}-affinity of the K299A mutant. The high Ca^{2+}-affinity in the two other mutants is likely linked to the observed loss of allosteric communication. Hence, our data suggest that the allosteric network in Langerin downregulates Ca^{2+} affinity.

H294 is a key player in the allosteric network and couples the long and the short loop

Residue H294 is a key component of the allosteric network because it is a central node in all three mutual information graphs connecting the clusters of the small and long loop. Notably, mutating this amino acid affected many residues that were also affected by Ca^{2+} binding in

the WT (**Figure 5A, left**). To investigate the structural origin of these perturbations, we performed a chemical shift projection (CHESPA) analysis.[42] Fractional shifts of the equilibrium population towards the holo or apo form can be delineated by this analysis on a per-residue basis by magnitude and angle of the chemical shift change.

Table 1: Binding affinities of Langerin CRD to Ca^{2+} at pH 6 and pH 7 obtained by ITC and NMR measurements.

	ITC[§]		NMR	
Mutant	K_d (μM)	ΔG (kJ mol^{-1})$^{+}$	K_d (μM)	ΔG (kJ mol^{-1})$^{+}$
WT (pH 6)	800 ± 150*	-17.8 ± 34	620 ± 50*	-18.4 ± 1.0
WT (pH 7)	105 ± 15*	-22.9 ± 3.3	160 ± 30	-21.8 ± 3.4
Q239A (pH 6)	-	-	640 ± 40	-18.3 ± 1.0
K257A (pH 6)	200 ± 20	-21.2 ± 0.3	265 ± 30	-20.6 ± 1.7
D263A (pH 6)	-	-	620 ± 30	-18.4 ± 1.1
S265A (pH 6)	-	-	570 ± 30	-18.6 ± 0.8
H294A (pH 6)	125 ± 5	-22.4 ± 0.9	110 ± 10	-22.7 ± 0.8
H294A (pH 7)	35 ± 15	-25.5 ± 8.5	-	-
N297A	-	-	770 ± 30	-17.9 ± 0.5
K299A	-	-	210 ± 20	-21.1 ± 1.3

[+]Free energies were calculated according to the relation ΔG= RT ln K_d with R=8.1314 kJ mol^{-1} K^{-1} and T = 300 K.
*Error given as standard deviation of three independent measurements.
[§]Stoichiometry was set to 1 to determine K_d using a one-set-of-sites binding model.

The CHESPA analysis revealed a set of positive shifts along the WT apo-holo vector for the short loop region, whereas the residues flanking the long loop and the Ca^{2+} binding site shifted in the opposite direction indicating an overall decoupling of the two loops (**Figure 6A**). For the other mutants, however, no clear pattern could be derived, suggesting a more complex mechanism (**Figure S13**).

To further investigate the decoupling of the loops, we performed a 2 μs MD simulation of the apo and holo H294A mutant, respectively. The distance distributions between the two loops and the autocorrelation function of the distance time series were calculated (**Figure 6B-C**). The distributions of the four systems (apo and holo WT, apo and holo H294A) show three major maxima, which we denoted – going from smaller to larger distances - closed, intermediate, and open state. In the closed state, the two loops are in direct van-der-Waals contact. However, the relative populations of these maxima, in particular of the closed state, vary strongly between the four structures. In the holo H294A mutant, the closed state is not populated at all and the autocorrelation function decays much faster than in the other three systems. Thus, the ability to form the closed state seems to be essential for the coupling of the two loops.

Additionally, we noticed during our NMR titration experiments of the H294A mutant increased peak intensities and the appearance of several additional peaks (**Figure 6D**), which likely belong to unassigned residues in the long loop. Hence, the removal of H294 sidechain shifted the exchange regime of the long loop on the NMR timescale further substantiating that the dynamics of this region changed notably. Although we observed decreased chemical shift perturbations in the short loop region upon Ca^{2+} addition in the H294A mutant, the communication was not completely abrogated supporting the notion that the network is robust.[41] Mutual dependence graphs computed for the H294A mutant revealed a loss of correlated movement of the two loops, further evidencing that the decoupling of the loops is connected with the increased affinity for Ca^{2+} (**Figure 6E**). Taken together, MD and NMR showed partial decoupling of the loop motions upon H294 mutation, which results in increased mobility of the long loop and increased affinity towards Ca^{2+}.

H294 partially entails pH responsiveness

The prominent role of H294 in the allosteric network, its elevated affinity for Ca^{2+} at pH 6 and the strong pH dependency of Ca^{2+} binding in the WT led us to hypothesize that H294 is a pH sensor similar to H256 in ASPGR (Wragg and Drickamer, 1999). First, we calculated pK_a values for the apo and holo form using two orthogonal algorithms making use of representative MD snapshots (**Table S4**) awarding pK_a values close to 6 for both forms implying that approximately half the population is protonated at pH 6. To assess whether protonation of H294 was solely responsible for the pH-dependence of Ca^{2+} affinity, we determined the dissociation constants of the H294A mutant by ITC at both pH 6 (K_d = 125 ± 5 μM) and pH 7 (K_d = 36 ± 15 μM) (**Figure S14A**). Moreover, comparison of the chemical shifts of both holo and apo form at

pH 6 and 7 shows that the pH responsiveness in the short loop in the holo form is conserved in absence of the H294 sidechain (**Figure S14B**). Both findings showed that H294 side chain is not the sole pH sensor. However, comparing the pH-dependent affinity increase of both WT and mutant revealed that the WT is more pH responsive than the mutant implying a partial contribution of H294 to the pH effect.

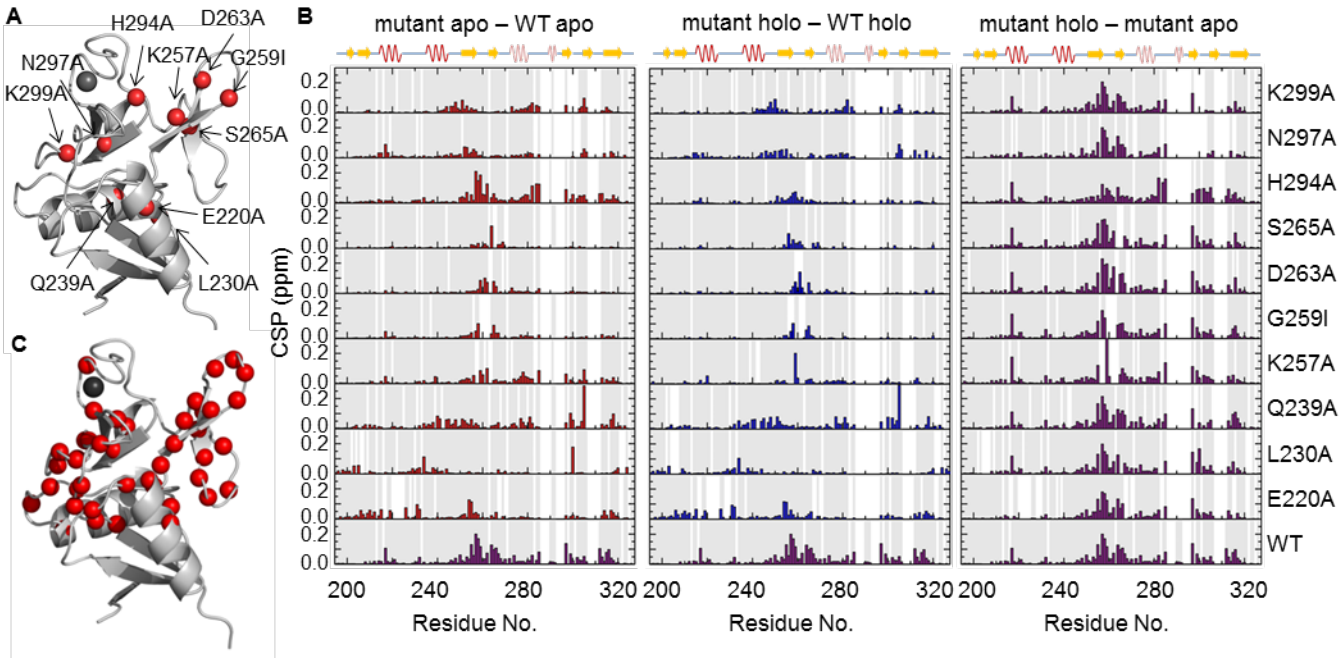

Figure 5: Single-residue mutations in Langerin CRD induce pronounced chemical shift changes remote from the mutation site. (A) Cartoon representation of Langerin CRD (pdb entry: 3P5F) with the mutated residues shown as red spheres and Ca^{2+} ion in grey. (B) CSP of mutant apo and holo forms (left and right panel) compared to the WT show a distinct CSP pattern. Bottom row shows the WT binding to Ca^{2+}.CSPs of the mutants upon addition Ca^{2+} (right panel) show a high conservation of the WT pattern except in K257A and H294A. Assigned residues are highlighted grey. All data was recorded at pH 6, 298 K. (C) Cartoon representation of the Ca^{2+} interaction network shown as red spheres and the Ca^{2+} ion in grey.

We used MD simulation of the apo protein with protonated H294 (apo cis H294+) to gain more insight into the pH effect. The side chain of H294 forms a hydrogen bond with the side chain of K257 in the small loop, which was populated in about 30 to 35% in the three WT simulations (apo trans WT, apo cis WT, holo cis WT). It is backed up by a second hydrogen bond from the backbone amide hydrogen of K257 to the carboxyl oxygen of H294, which is populated 51%-56% in the three WT simulations. (**Figure 6F, Table S1**). Our MD simulations of apo cis H294+ showed that the side chain hydrogen bond is indeed disrupted but the backbone hydrogen bond was maintained. Moreover, since both side chains of K257 and H294 are protonated in apo cis H294+, the two loops experience a Coulomb repulsion and are pushed apart (**Figure 6E**), which can be observed in the drastically altered distance distribution of the two loops for apo cis H294+ (**Figure 6B**). In particular, the closed state is not visited at all and the two loops do not seem to be in direct van-der-Waals contact. Correspondingly, the autocorrelation function differs from those of the WT and H294A mutant structures (**Figure 6C**). The initial decay is more pronounced after which the autocorrelation function decays relatively slowly with a timescale of 5.8 ns. Thus, protonation of H294 strongly changes the conformations and the dynamics of the two loops. Notably, this was much stronger due to protonation of H294 than the H294A mutation. Thus, we conclude that the contribution of H294 to the pH sensitivity of Langerin is predominantly caused by the presence of a second positive charge between the loops and not by the disruption of the hydrogen bond.

Finally, we noted that the WT and H294A holo chemical shifts were almost completely overlapped at pH 7 (**Figure 6G**), which was not the case at pH 6 (**Figure 4, middle**). This is a strong indicator for structural similarity of the WT and the H294A mutant at pH 7 and a further evidence for a pH-sensitive component encoded in the allosteric network independent from H294.

The allosteric network destabilizes the holo state with decreasing pH

To dissect the contributions of the single components to the pH-dependent regulation of Ca^{2+} binding by the allosteric network, we constructed a thermodynamic model based on the free energies differences of Ca^{2+} binding in the WT and in the mutants at both pH 6 and 7 (**Table 1, Figures 7 and S14A,C**). We calculated the free energy differences that range from -17.8 kJ mol^{-1} in WT at pH 6 to -25.5 kJ mol^{-1} in H294A at pH 7. Our analysis showed that the pH sensitivity of the Ca^{2+} affinity in WT Langerin (in total $\Delta\Delta G$ 5.1 kJ mol^{-1}) is a combination of two pH sensors: H249 and an unknown sensor. The pH-sensitivity of the H294A mutant is hence only due to the second pH sensor and amounts to $\Delta\Delta G$ 3.1 kJ mol^{-1}. Consequently, the contribution of H294 to the pH sensitivity in WT Langerin is 2 kJ mol^{-1}.

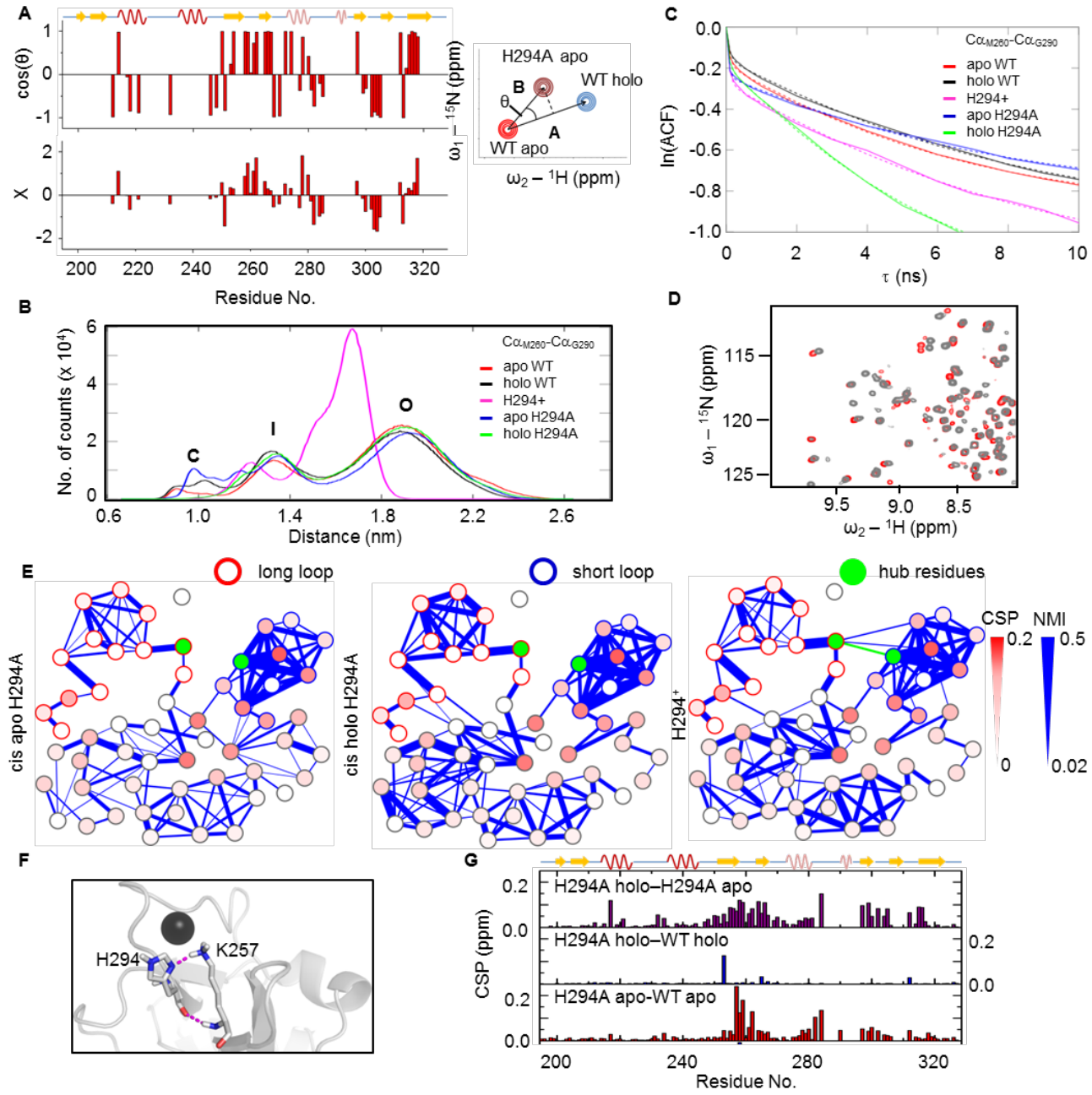

Figure 6: H294A mutant of Langerin CRD alters dynamics of the apo form and decouples the long and short loop. (A) CHESPA analysis of H294A apo at pH 6. Most changes induced by the mutation align very well with the reference vector ($|\cos(\theta)|\approx 1$, upper panel). Lower panel shows the projection of the vector lengths. (B) The short loop can adopt three distinct conformational states as monitored by the distance between the Cα-atoms of M260 and G290: closed (C), intermediate (I), and opened (O). (C) Autocorrelation functions (ACF) computed for same distance as in (B) (dashed line: double-exponential fit). The ACF of the holo H294A mutant showed the fastest decay (3.9 ns), suggesting a decoupling of the correlated movement of the two loops. (D) Overlay of ^{1}H-^{15}N HSQC NMR spectra of the apo forms of WT and H294A CRD at pH 6, 298 K. The mutant spectrum resolves additional peaks likely being the previously unassigned residues of the long loop. (E) Mutual dependence graphs computed for residues 255-310 of H294A cis apo (left panel) and cis holo (center panel), and cis apo WT with protonated H294 side chain (right panel). The hub residues H294 and K257 are highlighted in green. Mutation of H294 led to the loss of correlated movement along H294-K257 axis. (F) Two hydrogen bonds connect the hub residues K257, and H294, coupling the movement of the two loops. (G) NMR chemical shift perturbations of WT and H294A at pH 7. While the mutant and WT apo forms still differ, the holo forms have identical structures.

The overall Ca^{2+} affinity in the H294A mutant is increased compared to WT Langerin. We attributed this increase to the disruption of the allosteric network and estimate its magnitude to ΔΔG 4.6 kJ mol^{-1}. For the K257A mutant, this effect amounts to ΔΔG 2.8 kJ mol^{-1}, which leaves an unexplained difference to the H294A mutant of ΔΔG 1.8 kJ mol^{-1}. Allosteric communication is based on a multitude of physical interactions: presence and relative population of hydrogen bonds, presence and positions of charges, van-der-Waals contacts, loop flexibility etc. To dissect the individual contributions of these interactions to the allosteric network requires the detailed investigation of a series of mutants at various pH values. However, we can speculate that the second pH sensor is a protonation site in the vicinity of the Ca^{2+} binding site. In the K299A mutant at pH 6, this site is protonated but by removing the charged lysine at position 299 the effect of this second pH sensor muted. Thus, compared to WT Langerin at pH 6, the Ca^{2+} affinity K299A at pH6 should be increased (ΔΔG 3.1 kJ mol^{-1}). This is in very good agreement with the measured binding constant. But again detailed analysis of other mutants and pH values is needed to test this hypothesis. Finally, Q239 is not part of the allosteric network and far away from the binding site. The mutant Q239A serves as control and should behave as the WT Langerin. Indeed the Ca^{2+} binding constants only differ by 0.5 kJ mol^{-1}, which is within the experimental accuracy. This also confirms that the increase in binding constants in H294A and K257A is in fact due to the disruption of the allosteric network and not an artifact of the mutation itself.

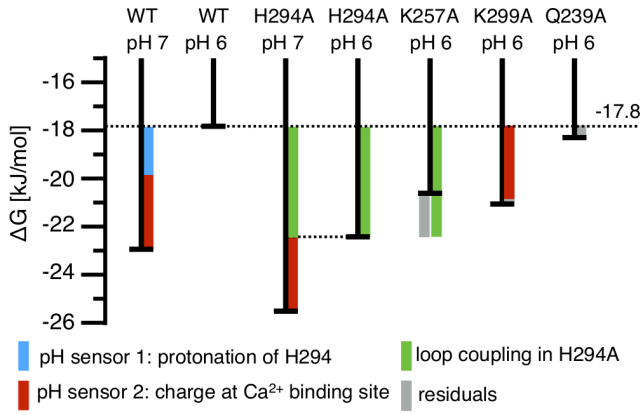

Figure 7: Contributions to the Ca2+ binding free energies in WT, H294A, K257A, K299A and Q239A.

Discussion

Langerin is an endocytic receptor that serves as a pattern recognition receptor initiating the immune response to invading pathogens. To further our insight into the underlying molecular mechanisms of cargo binding and release, Langerin resembles a good model. Our results reveal the absence of inter-domain allosteric communication between the CRDs for interactions with monovalent ligands as previously observed for DC-SIGN and DC-SIGNR[43] allowing for the isolated study of the CRD using NMR spectroscopy. Hence, we were able to identify Ca^{2+} affinity and its pH sensitivity as the two major contributors of ligands release.

Under extracellular conditions, pH 7 and 1 to 2 mM Ca^{2+} concentration, Langerin has a high affinity for Ca^{2+} shifting the binding equilibrium almost completely to the holo state, an observation in line with other CLTRs.[8] Upon acidification to pH 6 resembling the milieu of the early endosomal compartment, the affinity for Ca^{2+} decreases significantly thus favoring ligand release. For the mannose-binding protein a kinetic trap mechanisms based on the very slow prolyl bond isomerization of the central proline residue was suggested that prevents rebinding of the cargo to a recycling receptor.[12] Remarkably, a unique feature of Langerin is its high (75%) pH-independent cis prolyl bond conformation in the absence of Ca^{2+}. This degree of pre-organization of the long loop harboring the central proline is high compared to other CLRs where only 10% were reported for Tetranectin.[8,11-14] Hence, kinetically trapping the receptor in an binding-incompetent state is seemingly not at play for Langerin and rebinding to the recycling receptor is likely prevented by decreased Ca^{2+} affinity and potentially active Ca^{2+} export in the early endosome.[44]

Surprisingly, our analysis provided evidence from complementary methods for the existence of an extended allosteric network of communication amino acid side chains. NMR chemical shift perturbations of backbone resonances of Langerin by Ca^{2+} titration are located in sites distal from the actual Ca^{2+} recognition site suggesting a propagation of conformational changes in Langerin upon cofactor binding. Conversely, perturbing these remote sites using single point mutations caused these changes to propagate along the same routes through the protein similar to other allosteric proteins.[41] None of the single point mutations was able to completely abrogate the network suggesting that it is robust.[41] Moreover, our mutant analysis then unraveled a core network of amino acids, which is evolutionary conserved in Langerin. These data are substantiated by an extensive analysis of several microsecond molecular dynamics simulations using mutual information theory. Taken together, NMR, molecular dynamics simulations and evolutionary considerations led to the identification of an allosteric network in Langerin being associated with Ca^{2+} binding.

Among the mutations, H294A turned out to be particularly informative revealing that the network couples the mobility of the short and the long loop thereby weakening Ca^{2+} affinity, possibly by slowing down the motion of the long loop. Strikingly, the magnitude of correlated mobility observed per residue decreased from the trans to the cis apo state, being even further decreased in the holo form (**Figure 4**). These data suggest that the allosteric communication is impaired upon Ca^{2+} binding. Upon mutation of either H294 or its direct interaction partner K257, loop coupling is decreased and Ca^{2+} affinity is increased. We propose that the coupling of the loops restrains the long loop close to the short loop and upon decoupling, the long loop has improved Ca^{2+} coordination (**Figure S16).** Notably, K257 and H294 side chains highly

overlap with the Ca^{2+}-1 and -3 site of DC-SIGN, a related endocytic CLR (**Figure S17**). These data hint for an evolutionary mechanisms to substitute for the charge effects introduced by the allosteric Ca^{2+} ions in other CLRs that fine tune affinity for the primary Ca^{2+}. Hence, the allosteric network fulfills now this function of fine tuning the affinity, a hypothesis currently under investigation in our laboratories.

We further attempted to identify the pH dependent mechanism for Ca^{2+} release. As H294 was identified as a central player of the network, we asked whether its protonation state might serve as a regulator in analogy to the ASGPR, a hepatic CLR for which H202 was previously reported to play such role.[9] Our MD simulation suggested that H294 protonation at least partially decouples the loop dynamics (**Figure 6B**). To further delineate the pH-dependent and -independent contributions to Ca^{2+} affinity, we constructed a thermodynamic model based on the affinities of the WT and mutant data at both pH 6 and 7 (**Figure 7**, **Table 1**). Strikingly, H294 only partially contributes to the pH dependence of the Ca^{2+} affinity as could be seen from the persisting pH dependence of the H294A mutant. Other potential pH sensors are the members of the Ca^{2+} cage E285, E293, D308 for which remarkably high pK_a values were calculated (**Figure S18, Table S4**). In particular, the former two residues show similarity to an aspartyl dyad with elevated pK_a values similar to residues found in BACE-1 and HIV-1 protease.[45,46]

Several physical interactions change upon protonation of H294: (1) the side-chain hydrogen bond to K257 is broken, (2) the dynamics of the long loop and the short loop is decoupled, (3) a second positive charge is introduced between the two loops leading to a strong Coulomb repulsion between K257 and H294. Not all of these changes necessarily decrease the Ca^{2+} affinity, but the overall change in Ca^{2+} affinity seems to be in subtle balance between opposing effects. It is difficult to probe these effects individually, since mutating one of the interaction partners, K257 or H294, also affects the reference state at pH 7. In particular, the loops are at least partially decoupled in the two mutants. Moreover, the direct van-der-Waals contact between the side-chains of K257 and H294, which stabilizes the closed conformation of the loops in the WT at pH 7, is perturbed upon mutation, thereby introducing a fourth effect. Finally, K257A and H294A differ in their charge states, as K257 is protonated at pH7 and pH6, whereas H294 can only be protonated at pH 6. This likely explains the observed differences in Ca^{2+} affinity in the two mutants.

Additionally to these insights into the role of the allosteric network, we were also able to dismiss potential functions. First of all, we did not observe any marked difference of the cis/trans prolyl bond isomerization of the CRD at pH 6 for any mutant (**Table S3**), rendering this isomerization a network-independent conformational rearrangement. Moreover, the network is restricted to residues close to the ligand binding site, indicating that it is not involved in transmitting ligand binding information through the protein into the cell initializing cellular signaling pathways.[36] Finally, as several carbohydrate binding proteins have been suggested to compensate loss of conformational entropy upon ligand binding by increasing conformational entropy at remote sites of the protein, we investigated such hypothesis using our models.[47-49] However, without additional data, which is beyond the scope of this work, no clear conclusions could be drawn.

Overall, Langerin experiences remarkable dynamics on various timescales as revealed by NMR and MD simulations. The receptor is rather rigid under extracellular conditions and its mobility is restricted to the coupled movement of the long and short loop, which likely resides on the nanosecond timescale as inferred from NMR measurements. Upon endocytosis and hence Ca^{2+} release, additional micro- to millisecond dynamics appear, inferred from our NMR relaxation experiments (**Figure 3E, Figure S6**). Similar observations have been reported for other CLRs.[10,13] The mobility on the pico- to nanosecond timescale of Langerin did not change under these conditions albeit the allosteric network resides in this motional regime being based on the correlated mobility of amino acid side chains. This suggests rather a change in correlated mobility than a change in dynamics. Finally, on the second timescale major rearrangements in form of cis/trans prolyl isomerization occur. The different equilibrium populations observed in other CLRs might entail regulatory functions complementing our picture of a receptor architecture that exquisitely adapted to its function as a PRR promoting antigen uptake and release.

ASSOCIATED CONTENT

Supporting Information.
The Supporting Information is available free of charge on the ACS Publications website at DOI:
Detailed experimental methods, supplementary figures (PDF).

AUTHOR INFORMATION

Corresponding Author

* christoph.rademacher@mpikg.mpg.de
* bettina.keller@fu-berlin.de

Present Addresses

[#]Present address: Max Delbrück Center for Molecular Medicine. Robert-Rössle-Str. 10, 13092 Berlin; Germany.

Author Contributions

[⊥]These authors contributed equally. All authors have given approval to the final version of the manuscript.

Notes

The authors declare no competing financial interest.

ACKNOWLEDGMENT

C.R. thanks the German Research Society (DFG) for an Emmy Noether fellowship (1944/2-1). B.G.K., S.A. and J.H. acknowledge the DFG collaborative research center SFB 765 for generous support. B.G.K., C.R. and J.H. also thank the Funds of the Chemical Industry (FCI). S.A. and B.G.K acknowledge the computer facilities of the Freie Universität

Berlin (ZEDAT) for computer time. C.R. and J.H. further thank the Max Planck Society. J.H. and C.R. wish to thank Professor Peter H. Seeberger for fruitful scientific discussions and Olaf Niemeyer for technical support. J.H. also thanks Daniel Tesolin and Jia Hui Li for their help in optimization of protein production.

ABBREVIATIONS

CRD, carbohydrate recognition domain; ECD, extracellular domain; DC-SIGN(R), Dendritic cell-specific intercellular adhesion molecule-3-grabbing non-integrin (related); NOE, nuclear Overhauser enhancement; CLR, C-type lectin receptor; NMI, normalized mutual information; CSP, chemical shift perturbations; MD, molecular dynamics; ASPGR, asialoglycoprotein receptor; ACF, autocorrelation functions; NMR, nuclear magnetic resonance; WT, wild type.

REFERENCES

(1) Osorio, F.; Reis e Sousa, C. *Immunity* **2011**, *34*, 651.

(2) Forni, D.; Cagliani, R.; Tresoldi, C.; Pozzoli, U.; De Gioia, L.; Filippi, G.; Riva, S.; Menozzi, G.; Colleoni, M.; Biasin, M.; Lo Caputo, S.; Mazzotta, F.; Comi, G. P.; Bresolin, N.; Clerici, M.; Sironi, M. *PLoS Genet.* **2014**, *10*, e1004189.

(3) Guo, Y.; Feinberg, H.; Conroy, E.; Mitchell, D. A.; Alvarez, R.; Blixt, O.; Taylor, M. E.; Weis, W. I.; Drickamer, K. *Nat. Struct. Mol. Biol.* **2004**, *11*, 591.

(4) Gramberg, T.; Soilleux, E.; Fisch, T.; Lalor, P. F.; Hofmann, H.; Wheeldon, S.; Cotterill, A.; Wegele, A.; Winkler, T.; Adams, D. H.; Pohlmann, S. *Virology* **2008**, *373*, 189.

(5) Wragg, S.; Drickamer, K. *J. Biol. Chem.* **1999**, *274*, 35400.

(6) Snyder, G. A.; Ford, J.; Torabi-Parizi, P.; Arthos, J. A.; Schuck, P.; Colonna, M.; Sun, P. D. *J. Virol.* **2005**, *79*, 4589.

(7) Tabarani, G.; Thepaut, M.; Stroebel, D.; Ebel, C.; Vives, C.; Vachette, P.; Durand, D.; Fieschi, F. *J. Biol. Chem.* **2009**, *284*, 21229.

(8) Onizuka, T.; Shimizu, H.; Moriwaki, Y.; Nakano, T.; Kanai, S.; Shimada, I.; Takahashi, H. *FEBS J.* **2012**, *279*, 2645.

(9) Feinberg, H.; Torgersen, D.; Drickamer, K.; Weis, W. I. *J. Biol. Chem.* **2000**, *275*, 35176.

(10) Probert, F.; Mitchell, D. A.; Dixon, A. M. *FEBS J.* **2014**, *281*, 3739.

(11) Ng, K. K.; Park-Snyder, S.; Weis, W. I. *Biochemistry* **1998**, *37*, 17965.

(12) Ng, K. K.; Weis, W. I. *Biochemistry* **1998**, *37*, 17977.

(13) Poget, S. F.; Freund, S. M.; Howard, M. J.; Bycroft, M. *Biochemistry* **2001**, *40*, 10966.

(14) Nielbo, S.; Thomsen, J. K.; Graversen, J. H.; Jensen, P. H.; Etzerodt, M.; Poulsen, F. M.; Thogersen, H. C. *Biochemistry* **2004**, *43*, 8636.

(15) Valladeau, J.; Ravel, O.; Dezutter-Dambuyant, C.; Moore, K.; Kleijmeer, M.; Liu, Y.; Duvert-Frances, V.; Vincent, C.; Schmitt, D.; Davoust, J.; Caux, C.; Lebecque, S.; Saeland, S. *Immunity* **2000**, *12*, 71.

(16) Romani, N.; Clausen, B. E.; Stoitzner, P. *Immunol. Rev.* **2010**, *234*, 120.

(17) de Witte, L.; Nabatov, A.; Pion, M.; Fluitsma, D.; de Jong, M. A.; de Gruijl, T.; Piguet, V.; van Kooyk, Y.; Geijtenbeek, T. B. *Nat. Med.* **2007**, *13*, 367.

(18) van der Vlist, M.; de Witte, L.; de Vries, R. D.; Litjens, M.; de Jong, M. A.; Fluitsma, D.; de Swart, R. L.; Geijtenbeek, T. B. *Eur. J. Immunol.* **2011**, *41*, 2619.

(19) Ng, W. C.; Londrigan, S. L.; Nasr, N.; Cunningham, A. L.; Turville, S.; Brooks, A. G.; Reading, P. C. *J. Virol.* **2015**, *90*, 206.

(20) de Jong, M. A.; Vriend, L. E.; Theelen, B.; Taylor, M. E.; Fluitsma, D.; Boekhout, T.; Geijtenbeek, T. B. *Mol. Immunol.* **2010**, *47*, 1216.

(21) Hunger, R. E.; Sieling, P. A.; Ochoa, M. T.; Sugaya, M.; Burdick, A. E.; Rea, T. H.; Brennan, P. J.; Belisle, J. T.; Blauvelt, A.; Porcelli, S. A.; Modlin, R. L. *J. Clin. Invest.* **2004**, *113*, 701.

(22) Hsu, T. L.; Cheng, S. C.; Yang, W. B.; Chin, S. W.; Chen, B. H.; Huang, M. T.; Hsieh, S. L.; Wong, C. H. *J. Biol. Chem.* **2009**, *284*, 34479.

(23) Chabrol, E.; Nurisso, A.; Daina, A.; Vassal-Stermann, E.; Thepaut, M.; Girard, E.; Vives, R. R.; Fieschi, F. *PLoS ONE* **2012**, *7*, e50722.

(24) Munoz-Garcia, J. C.; Chabrol, E.; Vives, R. R.; Thomas, A.; de Paz, J. L.; Rojo, J.; Imberty, A.; Fieschi, F.; Nieto, P. M.; Angulo, J. *J. Am. Chem. Soc.* **2015**, *137*, 4100.

(25) Thepaut, M.; Valladeau, J.; Nurisso, A.; Kahn, R.; Arnou, B.; Vives, C.; Saeland, S.; Ebel, C.; Monnier, C.; Dezutter-Dambuyant, C.; Imberty, A.; Fieschi, F. *Biochemistry* **2009**, *48*, 2684.

(26) Mc Dermott, R.; Ziylan, U.; Spehner, D.; Bausinger, H.; Lipsker, D.; Mommaas, M.; Cazenave, J. P.; Raposo, G.; Goud, B.; de la Salle, H.; Salamero, J.; Hanau, D. *Mol. Biol. Cell* **2002**, *13*, 317.

(27) Stambach, N. S.; Taylor, M. E. *Glycobiology* **2003**, *13*, 401.

(28) Idoyaga, J.; Cheong, C.; Suda, K.; Suda, N.; Kim, J. Y.; Lee, H.; Park, C. G.; Steinman, R. M. *J. Immunol.* **2008**, *180*, 3647.

(29) van der Vlist, M.; Geijtenbeek, T. B. *Immunol. Cell Biol.* **2010**, *88*, 410.

(30) Ward, E. M.; Stambach, N. S.; Drickamer, K.; Taylor, M. E. *J. Biol. Chem.* **2006**, *281*, 15450.

(31) Probert, F.; Mitchell, D. A.; Dixon, A. M. *FEBS J.* **2014**, *281*, 3739.

(32) Pederson, K.; Mitchell, D. A.; Prestegard, J. H. *Biochemistry* **2014**, *53*, 5700.

(33) Williamson, M. P. *Prog. Nucl. Mag. Res. Sp.* **2013**, *73*, 1.

(34) Feeney, J.; Batchelor, J. G.; Albrand, J. P.; Roberts, G. C. K. *J. Magn. Reson.* **1979**, *33*, 519.

(35) Zelensky, A. N.; Gready, J. E. *FEBS J.* **2005**, *272*, 6179.

(36) Drickamer, K.; Taylor, M. E. *Curr. Opin. Struct. Biol.* **2015**, *34*, 26.

(37) Feinberg, H.; Taylor, M. E.; Razi, N.; McBride, R.; Knirel, Y. A.; Graham, S. A.; Drickamer, K.; Weis, W. I. *J. Mol. Biol.* **2011**, *405*, 1027.

(38) Peng, J. W.; Wagner, G. *Biochemistry* **1995**, *34*, 16733.

(39) Bowman, G. R.; Geissler, P. L. *Proc. Natl. Acad. Sci. USA* **2012**, *109*, 11681.

(40) Keller, B.; Gattin, Z.; van Gunsteren, W. F. *Proteins* **2010**, *78*, 1677.

(41) Boehr, D. D.; Schnell, J. R.; McElheny, D.; Bae, S. H.; Duggan, B. M.; Benkovic, S. J.; Dyson, H. J.; Wright, P. E. *Biochemistry* **2013**, *52*, 4605.

(42) Selvaratnam, R.; VanSchouwen, B.; Fogolari, F.; Mazhab-Jafari, M. T.; Das, R.; Melacini, G. *Biophys. J.* **2012**, *102*, 630.

(43) Coombs, P. J.; Harrison, R.; Pemberton, S.; Quintero-Martinez, A.; Parry, S.; Haslam, S. M.; Dell, A.; Taylor, M. E.; Drickamer, K. *J. Mol. Biol.* **2010**, *396*, 685.

(44) Gerasimenko, J. V.; Tepikin, A. V.; Petersen, O. H.; Gerasimenko, O. V. *Curr. Biol.* **1998**, *8*, 1335.

(45) Yamazaki, T.; Nicholson, L. K.; Wingfield, P.; Stahl, S. J.; Kaufman, J. D.; Eyermann, C. J.; Hodge, C. N.; Lam, P. Y. S.; Torchia, D. A. *J. Am. Chem. Soc.* **1994**, *116*, 10791.

(46) Kim, M. O.; Blachly, P. G.; McCammon, J. A. *PLoS Comp. Biol.* **2015**, *11*, e1004341.

(47) Diehl, C.; Engstrom, O.; Delaine, T.; Hakansson, M.; Genheden, S.; Modig, K.; Leffler, H.; Ryde, U.; Nilsson, U. J.; Akke, M. *J. Am. Chem. Soc.* **2010**, *132*, 14577.

(48) MacRaild, C. A.; Daranas, A. H.; Bronowska, A.; Homans, S. W. *J. Mol. Biol.* **2007**, *368*, 822.

(49) Nesmelova, I. V.; Ermakova, E.; Daragan, V. A.; Pang, M.; Menendez, M.; Lagartera, L.; Solis, D.; Baum, L. G.; Mayo, K. H. *J. Mol. Biol.* **2010**, *397*, 1209.

Table of Contents artwork